Strain hardening and plastic instability properties of austenitic stainless steels after proton and neutron irradiation

T.S. Byun *, K. Farrell, E.H. Lee [1], J.D. Hunn, L.K. Mansur

Metal and Ceramics Division, Oak Ridge National Laboratory, Building 5500, P.O. Box 2008, MS-6151, Oak Ridge, TN 37831, USA

Abstract

Strain hardening and plastic instability properties were analyzed for EC316LN, HTUPS316, and AL6XN austenitic stainless steels after combined 800 MeV proton and spallation neutron irradiation to doses up to 10.7 dpa. The steels retained good strain-hardening rates after irradiation, which resulted in significant uniform strains. It was found that the instability stress, the stress at the onset of necking, had little dependence on the irradiation dose. Tensile fracture stress and strain were calculated from the stress–strain curve data and were used to estimate fracture toughness using an existing model. The doses to plastic instability and fracture, the accumulated doses at which the yield stress reaches instability stress or fracture stress, were predicted by extrapolation of the yield stress, instability stress, and fracture stress to higher dose. The EC316LN alloy required the highest doses for plastic instability and fracture. Plastic deformation mechanisms are discussed in relation to the strain-hardening properties of the austenitic stainless steels. © 2001 Elsevier Science B.V. All rights reserved.

1. Introduction

The mercury target container vessel of the Spallation Neutron Source (SNS) and its surrounding water-cooled shroud will be exposed to intense fluxes of protons and spallation neutrons [1–3]. It is estimated that the container vessel will undergo radiation damage up to 10 displacements per atom (dpa) and the nuclear transmutation rates will be orders of magnitude larger than in fission reactors. Some of the nuclear transmutation products, particularly hydrogen and helium, are known to exacerbate radiation effects on mechanical properties [4–7]. As part of a materials R&D program to qualify materials for the SNS facility, three polycrystalline austenitic stainless steels, EC316LN, HTUPS316, and AL6XN, have been irradiated and tested as candidate

materials for the target container [7–10]. Irradiation was performed at Los Alamos Neutron Science Center (LANSCE), Los Alamos National Laboratory, in beams of 800 MeV protons and spallation neutrons up to 10.7 dpa. Tensile testing was performed at room temperature and the engineering tensile data are reported elsewhere [10–12].

In the present work, the strain-hardening and plastic instability behaviors of the irradiated austenitic stainless steels are analyzed in detail. The mechanical property parameters such as yield stress, plastic flow power-law coefficients, strain-hardening rate, uniform strain, and plastic instability stress are obtained from the tensile curves, and the effects of radiation on those parameters are discussed. For the tensile mode, the fracture stress and fracture strain were calculated from the measured fracture load and the coefficients of the power-law flow curve. Estimates were also made for the fracture toughness and the doses to plastic instability and to fracture from the tensile test data. In the discussion, the high strain-hardening capability of the irradiated austenitic stainless steels at room temperature was explained by aspects of deformation twinning.

---

* Corresponding author. Tel.: +1-865 576 7738; fax: +1-865 574 0641.

E-mail address: byunts@ornl.gov (T.S. Byun).

[1] Present address: Honeywell Electronic Materials, 1349 Moffett Park Drive, Sunnyvale, CA 94089, USA.

Table 1
Compositions of austenitic stainless steels used in this work

Material	Composition (wt%)										
	Bal.	Ni	Cr	Mo	Mn	Si	C	N	Nb	V	Ti
EC 316LN	Fe	12.2	17.45	2.5	1.81	0.39	0.024	0.067			
AL6XN	Fe	24.0	20.5	6.3	0.40	0.40	0.02	0.22			
HTUPS 316	Fe	16.2	13.9	2.46	2.04	0.12	0.076	0.021	0.15	0.52	0.27

2. Experimental

In this study, three austenitic stainless steels, EC316LN, HTUPS316, and AL6XN, were tested and their strain-hardening and instability/failure behaviors were investigated. The EC316LN alloy was included because Type 316LN stainless steel is the primary candidate material for the mercury container vessel of the SNS facility [9–14]. The EC316LN alloy for this experiment was the heat that has been studied extensively under neutron irradiation conditions in the international fusion reactor materials program. The two alternative candidate materials included for this experiment are the AL6XN alloy, a superstainless steel developed for high resistance to aqueous corrosion, and the HTUPS316 alloy (high temperature ultra-fine precipitate steel), a modified 316 stainless steel for high temperature application [15,16]. The chemical compositions and material identities of these are listed in Table 1. Flat miniature tensile specimens were used for the experiments, and one is sketched in Fig. 1. Its nominal gage section dimensions are 5 mm long, 1.2 mm wide, and 0.25 mm thick. All three austenitic steels were irradiated in annealed states. The EC316LN tensile specimens were annealed at 950 °C for 1 h in vacuum. The AL6XN and HTUPS316 specimens were annealed at 1110 °C for 30 min and at 1200 °C for 12 min, respectively, in helium, and then fast cooled.

The specimens were irradiated at different locations of the LANSCE accelerator target area for different irradiation exposures. The pulsed proton beam had an energy of 800 MeV and an average current of 1 mA. The time averaged maximum flux of the proton beam was 3.7×10^{14} p/cm^2 s and the accumulated on-line time was 3614 h. Table 2 contains irradiation data such as calculated dpa, He and H production rates, and measured proton and spallation neutron fluences. The gas production values are recommended only for relative comparisons because large errors and uncertainties exist in the computer code calculations [17]. It is expected that only part of the H concentrations produced is retained in the samples after escapes by recoil and diffusion during irradiation and storage for years and therefore the effect of H production on tensile test results is negligible [7]. More detailed descriptions on the fluence measurements and dpa and gas production calculations are found in references [11,17]. The average maximum temperature measured by thermocouples was in the range 60–160 °C during irradiation.

Tensile testing was performed at room temperature in a screw-driven tensile machine of the Advanced Technology Corporation (ATC) at a cross-head speed of 0.005 mm/s, corresponding to a nominal strain rate of 10^{-3} s^{-1}. A specially designed sliding carriage was used to protect the miniature specimens from accidental damage during remote handling into the testing machine, and to avoid deformation occurring outside the gage section at the pinholes during the test [11–14]. Load was applied under the shoulders through ledges machined into the sliding carriage, which were shaped to match the radius of the specimen shoulders. True stress–true strain curves were calculated from the load-displacement data to analyze the strain hardening characteristics and to estimate additional data such as fracture toughness and the doses to plastic instability and fracture. Note that the displacement measurements contained contributions from the stiffness of the testing machine and specimen carriage but, for simplicity, calculations were made without compensation.
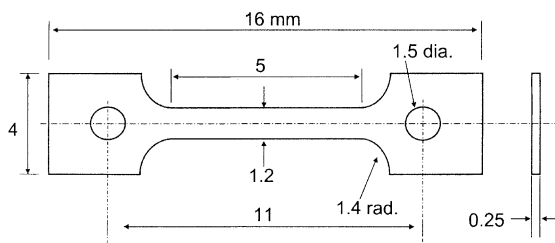
3. Strain-hardening properties

Figs. 2–4 presents the true stress (α)–true strain (ε) curves of the three test materials calculated from the load-displacement curves in the uniform deformation range. Corresponding engineering stress–strain curves are found in references [11,12]. Small yield point drops less than 20 MPa and short plateaus were found in the intermediate dose range 0.4–4 dpa. Smooth transitions

Fig. 1. Dimensions of miniature tensile specimen.

Table 2
Irradiation conditions for tensile specimens

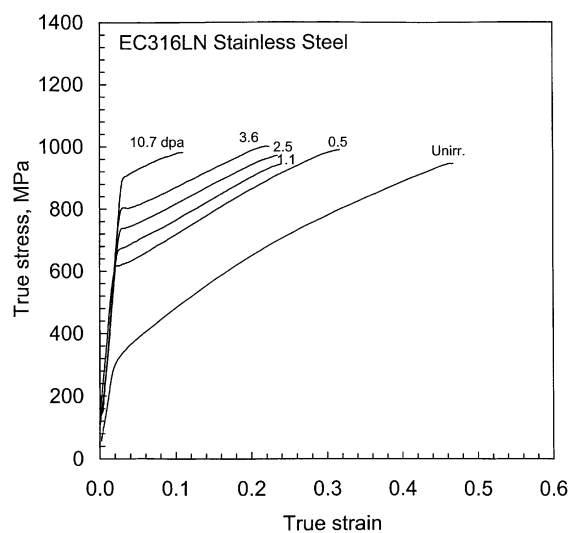| ID mark	Material	Irradiation temperature (°C)	Dose (dpa)	He (appm)	H (appm)	Proton fluence (p/cm²)	Neutron fluence (n/cm²)
E7	316LN	73–83	0.5	17	150	1.1E + 20	3.3E + 20
E8	316LN	73–83	0.7	31	260	2.5E + 20	3.9E + 20
E1	316LN	117–160	0.9	53	447	2.3E + 20	3.0E + 20
E4	316LN	58–67	1.1	58	518	2.6E + 20	4.6E + 20
E9	316LN	73–83	1.4	77	665	4.3E + 20	4.4E + 20
E2	316LN	117–160	2.4	152	1299	6.5E + 20	5.1E + 20
E5	316LN	58–67	2.5	146	1330	6.0E + 20	5.3E + 20
E6	316LN	58–67	3.6	217	1965	9.7E + 20	5.9E + 20
E3	316LN	117–160	10.7	825	6997	3.5E + 21	1.1E + 21
H4	HT UPS	73–83	0.4	16	145	7.8E + 19	3.1E + 20
H5	HT UPS	73 83	0.6	26	225	1.8E + 20	3.7E + 20
H6	HT UPS	73–83	1.1	60	521	3.0E + 20	4.2E + 20
H1	HT UPS	58–67	1.2	63	561	2.9E + 20	5.0E + 20
H2	HT UPS	58–67	2.8	161	1464	6.6E + 20	5.8E + 20
H3	HT UPS	58–67	4.0	240	2169	1.1E + 21	6.4E + 20
X10	Al6XN	73–83	0.5	17	150	1.1E + 20	3.3E + 20
X11	Al6XN	73–83	0.7	31	260	2.5E + 20	3.9E + 20
X2	AL6XN	117–160	0.9	53	447	2.3E + 20	3.0E + 20
X7	Al6XN	58–67	1.1	58	518	2.6E + 20	4.6E + 20
X12	Al6XN	73–83	1.4	77	665	4.2E + 20	4.4E + 20
X3	AL6XN	117–160	2.4	152	1299	6.5E + 20	5.1E + 20
X8	Al6XN	58–67	2.5	146	1330	6.0E + 20	5.3E + 20
X9	Al6XN	58 67	3.6	217	1965	9.7E + 20	5.9E + 20
X5	AL6XN	117–160	10.7	825	6997	3.5E + 21	1.1E + 21

Fig. 2. True stress–true strain curves of EC316LN stainless steel after irradiation to labeled doses in a spallation environment.
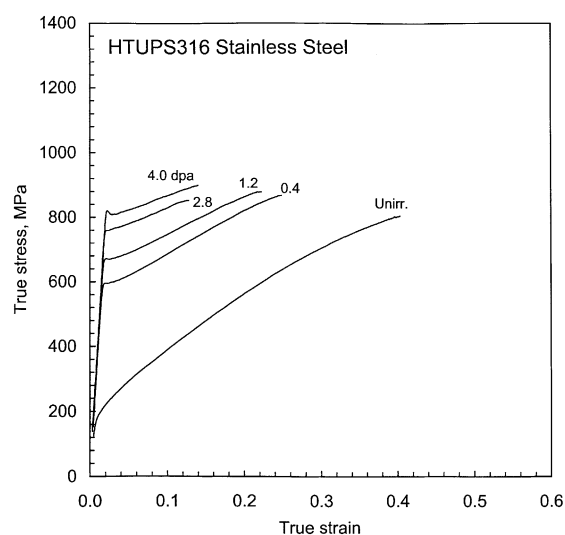

Fig. 3. True stress–true strain curves of HTUPS316 stainless steel after irradiation to labeled doses in a spallation environment.

from elastic to plastic deformations occurred in unirradiated specimens. At the highest dose of 10.7 dpa the transitions were less pronounced. Fig. 5 shows the ra-

diation effect on the 0.2% offset yield stress. The yield stress increased rapidly in the low dose range 0–0.5 dpa and more slowly in the higher dpa range.
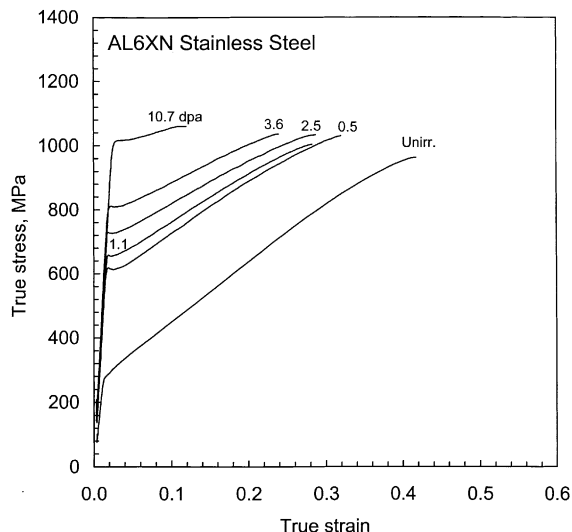
Fig. 4. True stress–true strain curves of AL6XN stainless steel after irradiation to labeled doses in a spallation environment.
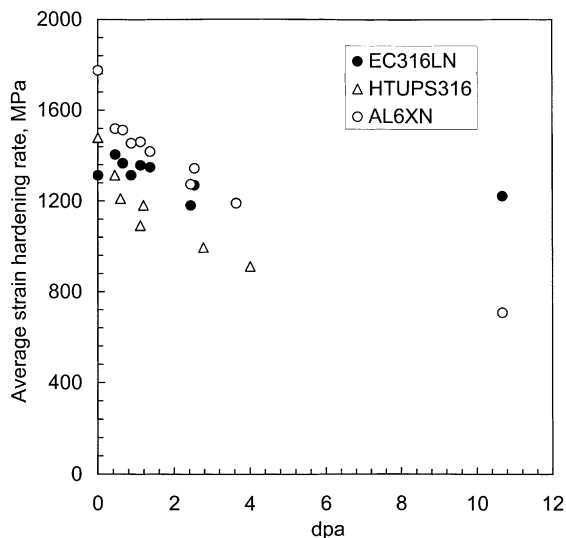

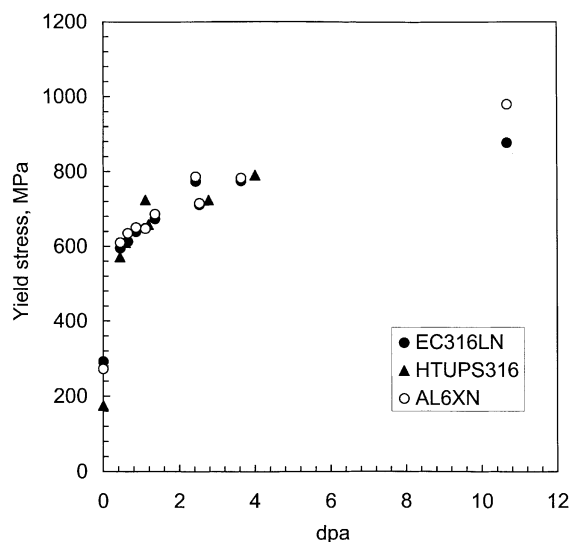Fig. 6. Variation of average strain-hardening rate with dpa.

Fig. 5. Variation of yield stress with dpa.

After the short plateaus, the stress–strain curves showed positive strain hardening until a plastic instability occurred at the uniform deformation limit (corresponding to the ultimate load). For the strain region above about 0.03, the strain-hardening rates ($d\sigma/d\varepsilon$) of unirradiated or low dpa specimens decreased with increasing strain, producing parabolic flow curves. However, the strain-hardening rates at higher doses were rather constant and thus formed nearly linear curves. The average strain-hardening rates over the uniform strain range are plotted in Fig. 6. In the dose range up to

3 dpa the AL6XN alloy showed the highest strain-hardening rate, while the HTUPS316 alloy showed the lowest value. The strain-hardening rate of these two alloys decreased more rapidly with increasing dpa than that of EC316LN alloy. The EC316LN alloy had medium values in the low dose range, but retained the highest strain-hardening rate of about 1200 MPa at the highest dose of 10.7 dpa. Overall, the three test materials showed strong strain-hardening capability over the dpa range.

In materials showing strain hardening, plastic instability or necking generally does not occur until the geometrical softening stress due to the decrease in load-carrying area becomes greater than the strain-hardening rate [18,19]. A high strain-hardening rate can homogenize plastic deformation over the gage section of specimen, and results in high uniform ductility. Therefore, the trend of decreasing strain-hardening rate with dose was repeated in the decrease of uniform strain with dose, as presented in Fig. 7.

Another interesting fact observed on the true stress–true strain curves is that the instability stress, which is defined as the true stress at ultimate load or at the onset of plastic instability, showed little dependence on dose. In the present work the instability stress is calculated by multiplying the ultimate tensile strength by the factor $\exp(\varepsilon_u)$, where ε_u is the uniform strain measured from the tensile curve [19]. Fig. 8 compares the variations of the instability stress with dpa for the three austenitic steels. The average instability stresses over the whole dose range were about 980, 850, and 1010 MPa for EC316LN, HTUPS316, and AL6XN alloys, respectively. As indicated in Figs. 2–4, the total strain hardening during uniform deformation decreased with
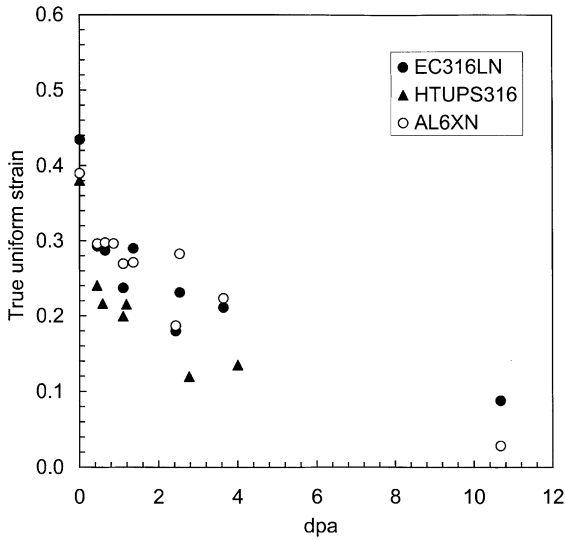
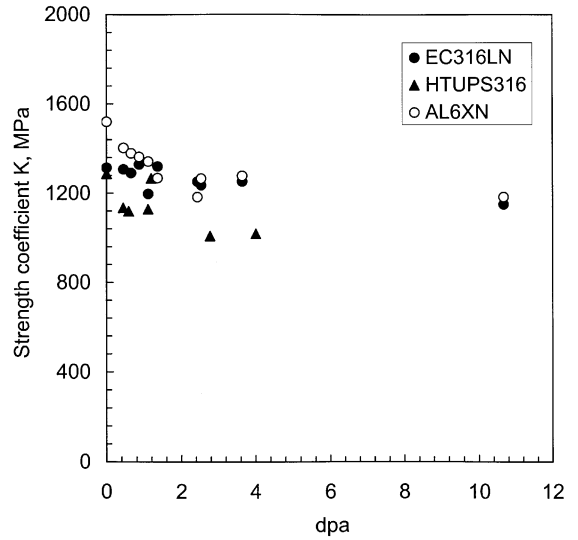Fig. 7. Variation of true uniform strain with dpa.

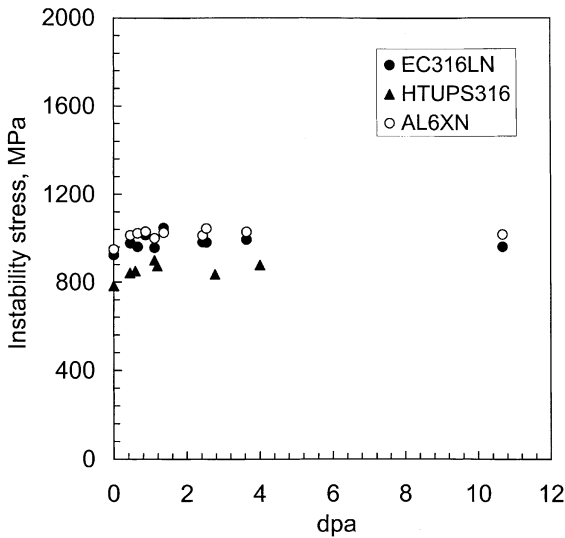Fig. 9. Variation of strength coefficient K with dpa.

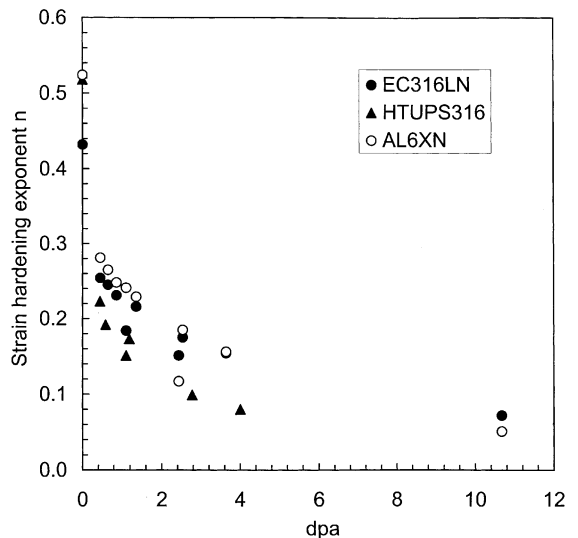

Fig. 8. Variation of instability stress with dpa.

Fig. 10. Variation of strain-hardening exponent n with dpa.

increasing dose, while the yield stress increased by a compensating amount, resulting in similar instability stresses for all doses.

Stress–strain data were fitted to a power-law curve: $\sigma = K\varepsilon^n$, where K is the strength coefficient and n the strain-hardening exponent. Figs. 9 and 10 show the radiation effects on the values of K and n. The strength coefficient K showed small dose dependence, while the strain-hardening exponent decreased rapidly with increasing dose. The values of the strain-hardening exponent are similar to the uniform strains, as can be predicted by Considere's instability condition:

$d\sigma/d\varepsilon = \sigma$, where σ is the true stress and ε the true strain [19].

4. Fracture parameters

Fracture strain and fracture stress were calculated from the fracture load measurements, P_F, and power-law flow curves described by K and n. After initiation of plastic instability, the deformation in the tensile specimen localizes, forming a neck. During necking a geometrical softening occurs in the load because the

cross-sectional area of the neck is reduced rapidly by the localized strain. Applying the condition of constant volume to the necking deformation, the minimum cross-sectional area of the neck at fracture, A_F, can be expressed as a function of fracture strain, ε_F [19]: $A_F = A_0 e^{-\varepsilon_F}$, where A_0 is the initial cross-sectional area of the specimen. Also, the fracture stress, σ_F, can be evaluated by the power-law curve: $\sigma_F = K\varepsilon_F^n$. Then, the fracture load, $P_F(= A_F\sigma_F)$, is expressed by

$$P_F = A_0 K \varepsilon_F^n e^{-\varepsilon_F}. \qquad (1)$$

Since the fracture load and flow curve coefficients are known, the above equation can be solved for the fracture strain, ε_F, by iterative calculations. Then, the fracture stress is calculated from the fracture strain and the coefficients of the power-law flow curve.

Fig. 11 shows the variations of fracture strain with dose for the three stainless steels. Large fracture strains of 0.89–0.95 were calculated for the unirradiated specimens. The fracture strain decreased with increasing dose, however, the EC316LN and AL6XN steels retained significant fracture strains in the dose range 0.4–10.7 dpa. The calculated values are consistent with the cross-sectional area reduction data measured on similar specimens of 304L and 316L stainless steels by Maloy et al. [20]. Fig. 12 presents the variations of fracture stress with dose. The fracture stress initially decreased with dose to 1–2 dpa, then become independent of dose. Among the three stainless steels the HTUPS316 alloy revealed the lowest level of fracture stress, although its yield stress was nearly the same as those of the other steels.

The fracture toughness was estimated from the tensile fracture strains and tensile fracture stresses using an
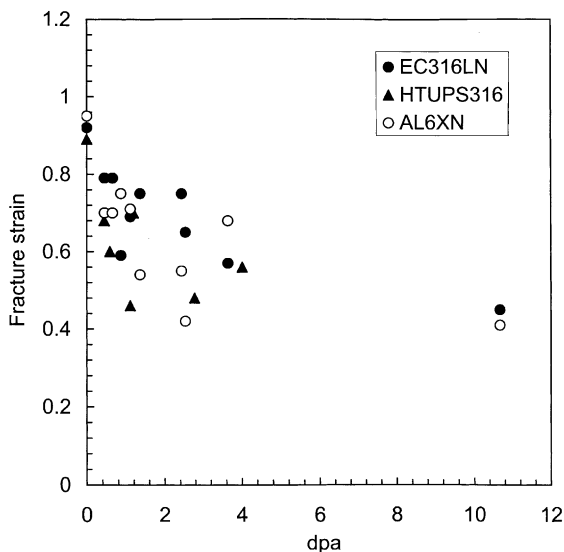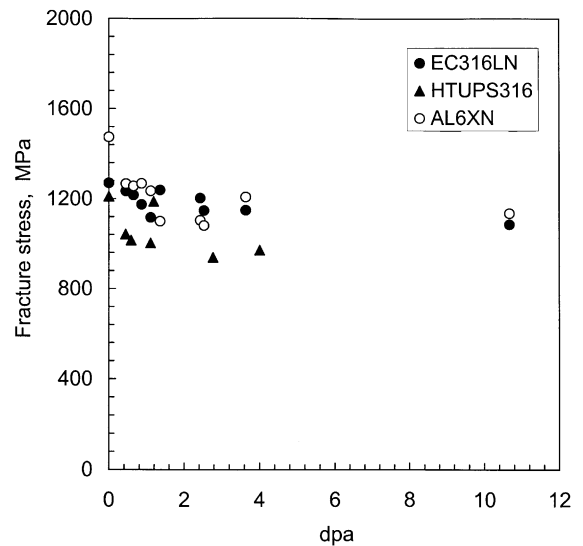

Fig. 12. Variation of fracture stress with dpa.

existing fracture toughness model. Work by Chen et al. [21] on a 304L stainless steel irradiated with 800 MeV protons showed that the fracture mode changed from ductile mode at 0.6 dpa to partial cleavage mode at 3.3 dpa and then to partial intergranular fracture mode at 7.8 dpa [21]. Since the dose range of the present experiment is similar to that experiment, the specimens of this study may have failed in ductile or mixed fracture modes depending on dose. During ductile or mixed mode fractures, most of the mechanical energy absorbed will be consumed by plastic deformation in the fracture process. For application to the test materials, therefore, a fracture toughness model considering fracture strain must be used. Hahn and Rosenfield [22] modified a critical fracture strain model to obtain an expression for fracture toughness, K_{IC}, in terms of ordinary tensile properties:

$$K_{IC} = 0.12\sqrt{E\sigma_{YS}\varepsilon_F(0.0005 + n^2)} \quad [\text{MPa}\sqrt{\text{m}}], \qquad (2)$$

where E is the Young's modulus, σ_{YS} the yield stress, ε_F the tensile fracture strain, and n the strain-hardening coefficient. The coefficient 0.12 was introduced on converting the British unit to the SI unit.

Fig. 13 presents the dose dependence of the fracture toughness estimated using Eq. (2). In unirradiated condition all the steels showed fairly high K_{IC} values in the range 300–450 MPa$\sqrt{\text{m}}$. A value of 355 MPa$\sqrt{\text{m}}$ was calculated for the EN316LN alloy. This value agrees well with Pawel et al. [23] experimental data for similar alloys; where 385, 393, and 360 MPa$\sqrt{\text{m}}$ were measured for EC316LN, J316, and JCPA alloys, respectively. Fig. 13 indicates that the irradiation resulted in a significant decrease in the fracture toughness. Among the three

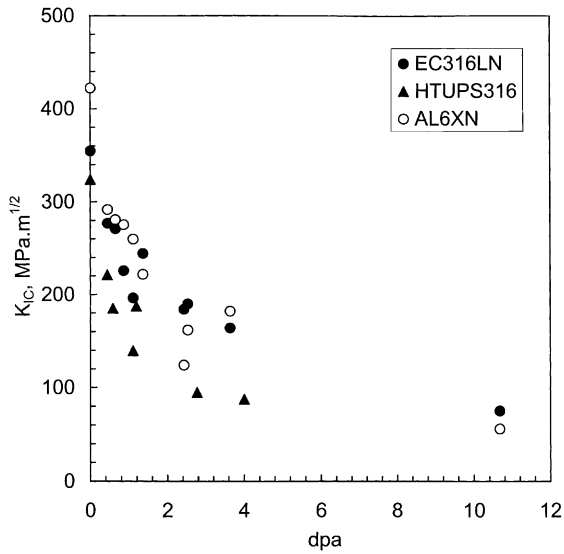Fig. 11. Variation of fracture strain with dpa.

Fig. 13. Variation of calculated fracture toughness with dpa.

alloys the HTUPS316 alloy showed the lowest fracture toughness level in both the irradiated and unirradiated conditions. Note that at the highest dose of 10.7 dpa a significant toughness of about 75 MPa$\sqrt{m}$ was still retained in the EC316LN alloy. This result agrees with the measured fracture toughness data for 304L and 316L stainless steels after irradiation in similar condition [24]. It should be pointed out, however, that the fracture toughness estimated from tensile properties, as above, may not correlate well with the data measured in a fracture toughness test when the material does not show significant plasticity before fracture at the test temperature.

5. Doses to plastic instability and fracture

Because the present stainless steels were irradiated and tested to supply changes in mechanical property data for reference in SNS target vessel design, estimations of service dose limits determined from the tensile test data would also be valuable. In this section, therefore, attempts to estimate the doses to plastic instability and fracture were made using the stress values obtained in the previous sections. As shown in Fig. 5, the yield stress increased rapidly with dose due to irradiation hardening, while the instability and fracture stresses were relatively insensitive to dose [25]. According to Considere's criterion, when the yield stress exceeds the instability stress, a necking or plastic instability will occur at yield. At a higher dose, when the yield stress reaches the fracture stress, the specimen would break at yield or fail in a non-ductile mode. On the stress versus

dpa plots the doses to plastic instability and fracture are defined as the dpa values at which the yield stress equals plastic instability stress and fracture stress, respectively. The yield stress, instability stress, and fracture stress were extrapolated to a higher dpa range to find intersections among the curves.

For the three steels, Figs. 14–16 present the relationships among the extrapolated curves of the yield stress, instability stress, and fracture stress for the three investigated steels. These stress-dose diagrams indicate
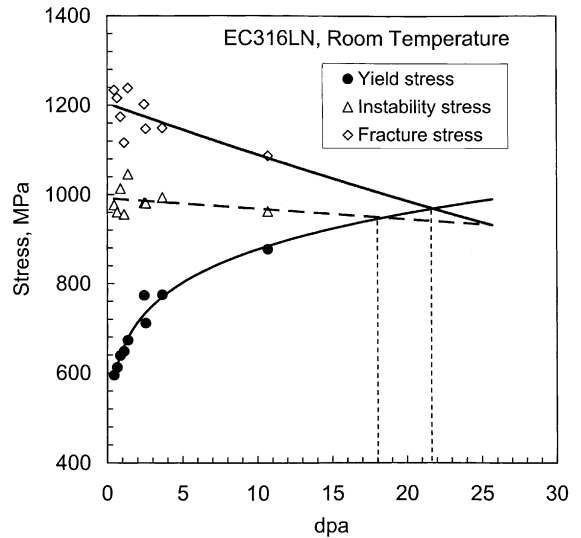

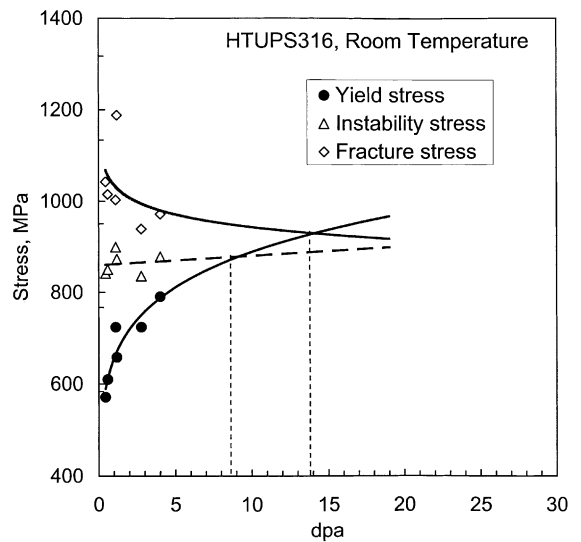Fig. 14. Prediction of lifetimes for EC316LN stainless steel at room temperature.

Fig. 15. Prediction of lifetimes for HTUPS316 stainless steel at room temperature.
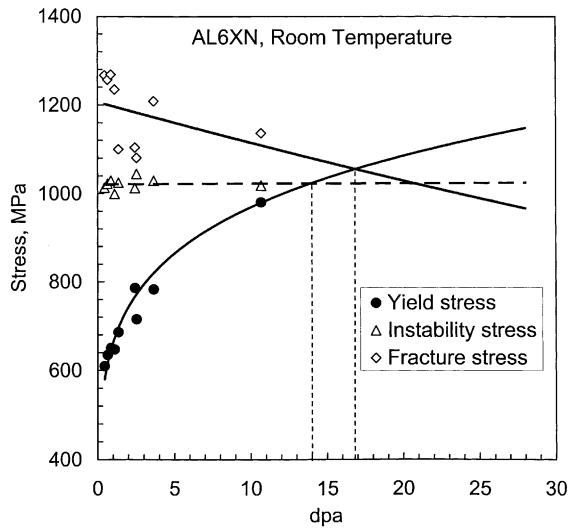
Fig. 16. Prediction of lifetimes for AL6XN stainless steel at room temperature.

Fig. 17. Prediction of lifetimes for 316L stainless steel at 164 °C.

that plastic instability will occur at yield after irradiation to about 5–20 dpa for tests at room temperature. The lowest dose for uniform deformation is predicted for the HTUPS316 alloy. As indicated in Fig. 5, similar yield stresses were measured for the three alloys. Therefore, the reason for the low dose to plastic instability of HTUPS316 alloy is because of its lower instability stress; the instability stress of the HTUPS316 alloy was about 150 MPa lower than those of the other two alloys. Among the three alloys, the EC316LN alloy is predicted to have the highest dose for deformation stability.

Similarly, the doses to fracture were predicted from the same Figs. 14–16. About 10–25 dpa were predicted for the three alloys. Again, the highest dose to fracture was predicted for the EC316LN alloy. Although similar instability stresses and fracture stresses are found in Figs. 8 and 12 for EC316LN and AL6XN alloys, larger dpa values to plastic instability and fracture are predicted for the EC316LN alloy. This is because the yield stress of the EC316LN alloy at 10.7 dpa is smaller than that of the AL6XN alloy, and thus the extrapolated curve for the yield stress of the EC316LN alloy is placed lower than that of the AL6XN alloy.

A stress-dose diagram was constructed also for a AISI 316L stainless steel tested at 164 °C [20], as presented in Fig. 17. This figure shows that the estimated dose to plastic instability is only about 4 dpa and that to fracture about 10 dpa. When compared with the room temperature case for EC316LN alloy in Fig. 14, much lower dose limits were predicted for this 164 °C case. Although there is a temperature difference of about 140 °C between the two cases, similar yield stresses of about 850 MPa at 8 dpa were obtained for both cases.
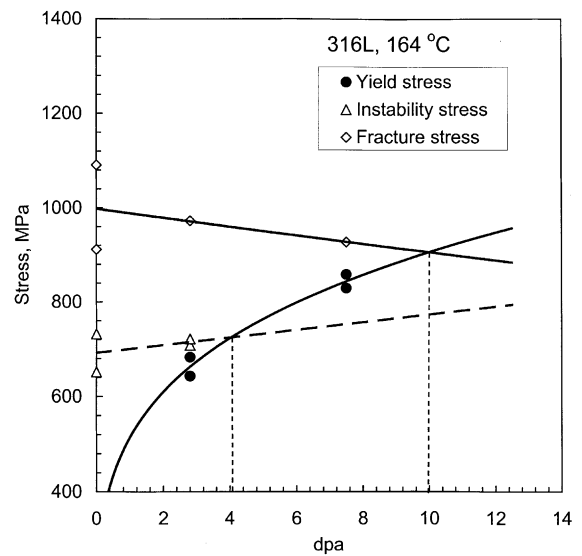
Therefore, the lower doses to instability and fracture for the 164 °C case are mainly because of its lower instability and fracture stresses. The instability stress of the AISI 316L alloy at 164 °C was calculated to be about 700 MPa, which is about 300 MPa lower than the value of the EC316LN alloy at room temperature. Also, if compared at the same dose, the fracture stress of the AISI 316L alloy at 164 °C is about 200 MPa lower than that of the EC316LN alloy at room temperature. The difference between the instability stress and the fracture stress for AISI 316L steel at 164 °C is at least 1.5 times higher than the corresponding differences for our steels at room temperature. Since the stress difference is the hardening stress during necking, we can deduce that much higher plasticity is introduced to the necked region before fracture at 164 °C than at room temperature. This higher necking ductility resulted in significant fracture toughness at 164 °C after irradiation even though the engineering tensile curve showed prompt necking at yield [20].

6. Discussion of deformation mechanism and strain-hardening rate

Pronounced reduction in strain-hardening rate is a common phenomenon for many irradiated materials [12–14,25–28]. As indicated in Figs. 6 and 8, however, all the irradiated austenitic steels retained significant strain-hardening rates during deformation at room temperature. Such hardening capabilities resulted from the characteristic deformation mechanism of the austenitic

steels. Dislocation slip and mechanical twinning are known as the most important deformation mechanisms for both unirradiated and irradiated stainless steels [29–37]. Usually, dislocation glide and deformation twinning in the austenitic steels are highly confined in the {1 1 1} slip planes [38]. Some strain-induced martensite phase particles were found by other workers in the microstructures of material irradiated and deformed at low temperatures; however, the amount of the martensite phase was too small to be a major deformation product [36].

Comprehensive transmission electron microscopy (TEM) studies on the deformation microstructure have been performed by the authors on the test materials, or equivalent steels, after irradiation [30–35]. The results indicated that the present test materials deformed in a mechanical twinning mode after high dose irradiation and deformation at room temperature. Irradiation by He^+ ions enhanced the tendency of twinning during plastic deformation; the deformation microstructure changed progressively with irradiation from dislocation networks at low dose to channel bands consisting of twin layers, stacking faults, and piled-up dislocations at higher doses [31,32]. To simulate spallation irradiation conditions, EC316LN and AISI 316LN austenitic steel were irradiated up to 10 dpa by simultaneous Fe^+, He^+, and H^+ ion beams in the MeV range [33–35]. The Fe^+ beam introduced displacement damage into the steels and the He^+ and H^+ beams injected corresponding simulated spallation transmutation products at the appropriate relative rates. Deformation microstructures after the irradiation confirmed that twinning played a major role in the room temperature deformation of irradiated austenitic steels. Similar deformation microstructures consisting of twins and some martensite phase [36] were observed in neutron-irradiated austenitic stainless steels. All the above TEM results confirm that mechanical twinning enhanced by irradiation hardening concurs with the respectable strain-hardening rate of the irradiated austenitic stainless steels over uniform strain range [21,36].

Mechanical twinning, along with confinement of dislocation slip, is also responsible for the excellent ductility of austenitic stainless steels near room temperature or below [39]. A general trend found in most face-centered cubic materials is that ductility decreases as the test temperature decreases. For the austenitic stainless steels, however, higher strain-hardening rate and ductility are measured at low temperatures than at elevated temperatures. In the temperature range of around room temperature to 200 °C, both ductility and strength increase as the temperature decreases [39,40]. The propensity for twinning and confinement of dislocation slip also increases as the test temperature decreases [29]. A ductility maximum exists at around room temperature or below.

Most aspects of mechanical twinning in the austenitic steels seem to be beneficial for a high strain-hardening capability [29]. First, the mechanical twinning in the austenitic steels is initiated by separation of a perfect dislocation into two partial dislocations and glide of the leading partial dislocation, forming a stacking fault between the leading and trailing partials [29,38]. Large pile-ups of partial dislocations were found in the deformation microstructures consisting of twin bands. Detailed analyses on TEM microstructures showed that the twins were formed by a progressive glide of Shockley partial dislocations, and many twin bands consisted of multiple thin twin layers [30–35]. Since the twinning can produce a high shear strain of 70.7% within the twin band [29], a significant macroscopic strain can be achieved by the twinning mechanism when massive twinning occurs at low temperatures or after irradiation in multiple slip systems. Also, the suppression of cross-slip due to the stacking faults would enhance the confinement of dislocation pile-ups to the easy glide slip planes and thus increases the strain-hardening rate due to the long-range back stresses from the pile-ups. The long-range back stress would encourage initiation of other bands in the same grain or adjacent grains, which results in higher ductility.

Secondly, the twinning generates internal barriers to slip and additional twinning [29,41]. The deformation twins in austenitic steels initiated mostly at grain boundaries and can extend from grain boundary to grain boundary [29]. Therefore, twin bands formed in the multiple slip systems break down the grain into smaller domains and act as planar barriers to additional deformation. This results in an increase in strain-hardening rate due to a boundary hardening effect [29]. Furthermore, the twin-matrix boundaries and the volume fraction of twin bands increase progressively as the strain increases. A large number of initial barriers can produce a high strain-hardening rate only at low strain, however, the progressively increasing number of barriers generated by deformation can extend high strain-hardening rate to higher strain levels, thus delaying plastic instability. Another aspect of the twins as barriers is that they are penetrable barriers in most of the temperature range, and the twin–twin penetrations can occur without causing micro-cracking [41]. At twin–twin intersections at a cryogenic temperature of −196 °C, where the twins were very thin and dislocation density was very low, micro-cracking was observed.

As mentioned previously, when compared with the EC316LN alloy at room temperature, about 30% lower instability stress was retained in the 316L alloy at 164 °C. At this elevated temperature both 304L and 316L stainless steels experienced necking prematurely [20], after irradiation to more than 4 dpa. Consequently, the uniform elongations were measured to be less than 1%. Hashimoto et al. [36] reported that a high

strain-hardening capability was retained due to twinning and martensite formation during deformation, while a negative slope on the engineering stress–strain curve resulted from channel formation. It is known that for austenitic stainless steels the critical stress for dislocation slip decreases with increasing test temperature, while the stress necessary for mechanical twining is less sensitive to the temperature [29]. Thus dislocation glide becomes more important at elevated temperatures. In face-centered cubic metals, slip bands are widened by cross-slip of screw dislocations at elevated temperatures [42]. Dislocation channeling in irradiated materials is also a widening process of slip bands [43–47]. Since the austenitic stainless steels have low stacking fault energies of $\simeq 10^{-2}$ J/m^2, cross-slip would not be favored at low temperatures because the wide stacking faults suppress the re-association of partial dislocations. At elevated temperatures, however, cross-slip can be activated and thus enhance the formation of channels [29]. Although twinning can produce 70.7% shear strain within the twin layer, only one partial dislocation can glide by one Burgers vector on each atomic plane. This would not be enough strain to remove all radiation-induced defects in a channel formed by twinning. Therefore, the reduction in strength would not be profound within the twin bands. However, when channels are formed by multiple glides of perfect dislocations, much higher shear strains, up to 400%, can be introduced within the channels [43–47]. In this channel the strain-hardening rate might be near zero or negative because the defects would be removed more thoroughly by multiple glides of channeling dislocations on the same plane [47].

7. Summary and conclusions

The strain-hardening behaviors and fracture parameters were analyzed for EC316LN, HTUPS316, and AL6XN austenitic stainless steels irradiated by 800 MeV protons and spallation neutrons up to 10.7 dpa at temperatures between 60 and 160 °C. The results are summarized as follows:

1. Although the austenitic stainless steels showed considerable irradiation hardening and loss of ductility, they retained good strain-hardening capability during deformation at room temperature. The high strain-hardening capability delayed plastic instability and resulted in a significant uniform strain after irradiation.

2. The instability stress showed little dependence on the irradiation dose. The average instability stresses over the dpa range were about 980, 850, and 1010 MPa for EC316LN, HTUPS316, and AL6XN alloys, respectively.

3. Tensile fracture stress and strain were calculated from the measurements of fracture load and stress–strain curve data. Also, the fracture toughness was estimated from those parameters using an existing model. The irradiation resulted in a significant decrease in the toughness value, however, the EC316LN alloy still retained a significant toughness of about 75 MPa$\sqrt{\text{m}}$ at 10.7 dpa.

4. The doses to plastic instability and fracture were predicted by extrapolation of the yield stress, instability stress, and fracture stress data to higher dose range. The EC316LN alloy showed the highest doses: about 18 dpa for plastic instability and about 22 dpa for brittle fracture. An AISI 316L alloy tested at 164 °C showed significantly lower doses to plastic instability and fracture due to its low plastic instability and fracture stresses.

5. Deformation mechanisms are discussed in relation to the strain-hardening properties of austenitic stainless steels. Mechanical twinning is believed to be responsible for the retained strain-hardening capability of austenitic stainless steels at room temperature.

References

[1] T.A. Gabriel, J.M. Barnes, L.A. Charlton, J. DiStefano, K. Farrell, J. Haines, J.O. Johnson, L.K. Mansur, S.J. Pawel, M. Siman-Tov, R. Taleyarkhan, T.J. McManamy, M.J. Rennich, in: Proceedings of the Topical Meeting on Nuclear Applications of Accelerator Technology, Albuquerque, New Mexico, November 16–20, 1997, American Nuclear Society, La Grange Park, IL, p. 288.

[2] J.R. Haines, T.A. Gabriel, T.J. McManamy, in: Proceedings of the Second International Topical Meeting on Nuclear Applications of Accelerator Technology, Gatlinburg, TN, September 20–23, 1998, American Nuclear Society, La Grange Park, IL, p. 222.

[3] L.K. Mansur, T.A. Gabriel, J.R. Haines, D.C. Lousteau, J. Nucl. Mater. 296 (2001) 1.

[4] M.S. Wechsler, M.H. Barnett, D.J. Dudjiak, L.K. Mansur, L.A. Charlton, J.M. Barnes, J.O. Johnson, in: Proceedings of the Symposium on Materials for Spallation Neutron Sources, Orlando, FL, Febrauary 9–13, 1997, The Miner-

als, Metals and Materials Society, Warrendale, PA, 1998, p. 23.

[5] E.J. Pitcher, P.D. Ferguson, G.J. Russell, R.E. Prael, D.G. Madland, J.D. Court, L.L. Daemen, in: Proceedings of the Symposium on Materials for Spallation Neutron Sources, TMS, Orlando, FL, Febrauary 10–12, 1997, p. 15.

[6] E.H. Lee, J.D. Hunn, T.S. Byun, L.K. Mansur, J. Nucl. Mater. 280 (2000) 18.

[7] J.D. Hunn, E.H. Lee, T.S. Byun, L.K. Mansur, J. Nucl. Mater. 282 (2000) 131.

[8] L.K. Mansur, J.R. Distefano, K. Farrell, E.H. Lee, S.J. Pawel, M.S. Wechsler, in: Proceedings of the Topical Meeting on Nuclear Applications of Accelerator Tech., Albuquerque, NM, November 16–20, 1997, American Nuclear Society, La Grange Park, IL, p. 301.

[9] L.K. Mansur, Trans. ANS 80 (1999) 94.

[10] K. Farrell, Spallation Neutron Source Project Report: SNS/TSR-0036, Oak Ridge National Laboratory, March, 1998.

[11] K. Farrell, T.S. Byun, Spallation Neutron Source Project Report: SNS/TSR-193, Oak Ridge National Laboratory, May, 2000.

[12] K. Farrell, T.S. Byun, in: J. Nucl. Mater. 296 (2001) 129.

[13] K. Farrell, T.S. Byun, J.W. Jones, L.T. Gibson, R.G. Sitterson, N. Hashimoto, J.L. Bailey, J. Gardner, in: Small Specimen Test Techniques, ASTM STP 1418, American Society for Testing and Evaluation, 2002, in press.

[14] K. Farrell, L.K. Mansur, in: L.K. Mansur, H. Ullmaier (Eds.), Proceedings of the International Workshop on Spallation Materials Technology, CONF-960451, Oak Ridge, April 23, 1996.

[15] P.J. Maziasz, R.W. Swindeman, J.P. Montage, M. Fitzpatrick, P.F. Browning, J.F. Grubb, R.C. Klug, Mater. High Temp. 16 (4) (1999) 207.

[16] P.J. Maziasz, J. Met. 41 (7) (1989) 14.

[17] M.R. James, S.A. Maloy, W.F. Sommer, P. Ferguson, M.M. Fowler, K. Corzine, in: Proceedings of the 2nd International Topical Meeting on Nuclear Applications of Accelerator Technology, Gatlinburg, TN, USA, September 20–23, 1998, American Nuclear Society, p. 605 (also, e-mail correspondence with M.R. James, S.A. Maloy, June 29, 1999).

[18] R.W. Hertzberg, Deformation and Fracture Mechanics of Engineering Materials, 3rd Ed., Wiley, New York, 1989, p. 20.

[19] G.E. Dieter, Mechanical Metallurgy, 3rd Ed., McGraw-Hill, New York, 1986, p. 283.

[20] S.A. Maloy, M.R. James, G. Willcutt, W.F. Sommer, M. Sokolov, L.L. Snead, M.L. Hamilton, F. Garner, J. Nucl. Mater. 296 (2001) 119.

[21] J. Chen, Y. Dai, F. Carsughi, W.F. Sommer, G.S. Bauer, H. Ullmaier, J. Nucl. Mater. 275 (1999) 115.

[22] G.T. Hahn, A.R. Rosenfield, in: Applications Related Phenomena in Titanium Alloys, ASTM STP 432, American Society for Testing and Evaluation, 1986, p. 5.

[23] J.E. Pawel, D.J. Alexander, M.L. Grossbeck, A.W. Longest, A.F. Rowcliffe, G.E. Lucas, S. Jitsukawa, A. Hishinuma, K. Shiba, J. Nucl. Mater. 212–215 (1996) 442.

[24] M.A. Sokolov, J.P. Robertson, L.L. Snead, D.J. Alexander, P. Ferguson, M.R. James, S.S. Maloy, W. Sommer, G. Willcutt, M.R. Louthan, in: Effects of Radiation Materials: 20th International Symposium, ASTM STP 1405, American Society for Testing and Evaluation, 2002.

[25] E.V. van Osch, M.I. DeVries, J. Nucl. Mater. 271&272 (1999) 162.

[26] S.M. Ohr, Scripta Metall. 2 (1968) 213.

[27] J.E. Pawel, A.F. Rowcliffe, D.J. Alexander, M.L. Grossbeck, K. Shiba, J. Nucl. Mater. 233–237 (1996) 202.

[28] G.E. Lucas, M. Billone, J.E. Pawel, M.L. Hamilton, J. Nucl. Mater. 233–237 (1996) 207.

[29] M.A. Meyers, K.K. Chawla. In: Mechanical Behavior of Materials, Prentice-Hall, Englewood Cliffs, NJ, 1998, p. 264.

[30] E.H. Lee, T.S. Byun, J.D. Hunn, N. Hashimoto, K. Farrell, J. Nucl. Mater. 281 (2000) 65.

[31] E.H. Lee, T.S. Byun, J.D. Hunn, L.K. Mansur, J. Nucl. Mater. 296 (2001) 183.

[32] E.H. Lee, T.S. Byun, L.K. Mansur, Acta Mater. (2001) in press.

[33] T.S. Byun, E.H. Lee, J.D. Hunn, K. Farrell, L.K. Mansur, J. Nucl. Mater. 296 (2001) 203.

[34] E.H. Lee, J.D. Hunn, N. Hashimoto, L.K. Mansur, J. Nucl. Mater. 278 (2000) 266.

[35] J.D. Hunn, E.H. Lee, T.S. Byun, L.K. Mansur, J. Nucl. Mater. 296 (2001) 203.

[36] N. Hashimoto, S.J. Zinkle, A.F. Rowcliffe, J.P. Robertson, S. Jitsukawa, J. Nucl. Mater. 283–287 (2000) 528.

[37] J.I. Cole, S.M. Bruemmer, J. Nucl. Mater. 225 (1995) 53.

[38] J.P. Hirth, J. Lothe. In: Theory of Dislocations, McGraw-Hill, New York, 1968, p. 288.

[39] Chromium-Nickel Stainless Steel Data, Data book of the International Nickel Company, New York, 1963.

[40] D.W. Kim, W.S. Ryu, J.H. Hong, S.K. Chi, J. Mater. Sci. 33 (1998) 675.

[41] P. Mullner, Mater. Sci. Eng. A 234–236 (1997) 94.

[42] R.W.K. Honeycombe, The Plastic Deformation of Metals, Edward Arnold, 1971, p. 80.

[43] M.S. Wechsler, The Inhomogeneity of Plastic Deformation, American Society of Metals, Metals Park, OH, 1971 (Chapter 2).

[44] J.V. Sharp, Acta Metall. 22 (1974) 449.

[45] J.V. Sharp, Philos. Mag. 16 (1967) 77.

[46] F.A. Smidt, Dislocation Channeling in Irradiated Metals, NRL Report 7078, Naval Research Laboratory, Washington, DC 20390, June 3, 1970.

[47] M.J. Makin, J.V. Sharp, Phys. Stat. Sol. 9 (1965) 109.